

Journal of Biomedical Optics

SPIEDigitalLibrary.org/jbo

Photoacoustic tomography of foreign bodies in soft biological tissue

Xin Cai
Chulhong Kim
Manojit Pramanik
Lihong V. Wang

Photoacoustic tomography of foreign bodies in soft biological tissue

Xin Cai, Chulhong Kim,* Manojit Pramanik, and Lihong V. Wang

Washington University in St. Louis, Department of Biomedical Engineering, Optical Imaging Laboratory, St. Louis, Missouri 63130

Abstract. In detecting small foreign bodies in soft biological tissue, ultrasound imaging suffers from poor sensitivity (52.6%) and specificity (47.2%). Hence, alternative imaging methods are needed. Photoacoustic (PA) imaging takes advantage of strong optical absorption contrast and high ultrasonic resolution. A PA imaging system is employed to detect foreign bodies in biological tissues. To achieve deep penetration, we use near-infrared light ranging from 750 to 800 nm and a 5-MHz spherically focused ultrasonic transducer. PA images were obtained from various targets including glass, wood, cloth, plastic, and metal embedded more than 1 cm deep in chicken tissue. The locations and sizes of the targets from the PA images agreed well with those of the actual samples. Spectroscopic PA imaging was also performed on the objects. These results suggest that PA imaging can potentially be a useful intraoperative imaging tool to identify foreign bodies. © 2011 Society of Photo-Optical Instrumentation Engineers (SPIE). [DOI: 10.1117/1.3569613]

Keywords: photoacoustic tomography; foreign body; soft tissue imaging.

Paper 10536PR received Sep. 30, 2010; revised manuscript received Feb. 20, 2011; accepted for publication Mar. 2, 2011; published online Apr. 18, 2011.

1 Introduction

Wounds, especially those inflicted by weapons or other explosions, may contain debris of various materials, such as glass, wood, cloth, plastic, and metal. Retained foreign bodies may cause inflammatory, allergic, and infectious complications.¹ Furthermore, the wounded tissue is devitalized. Treatment is more likely to work well when both foreign bodies and devitalized tissue are identified and removed early.² Current imaging modalities employed for detecting foreign bodies include x-ray computed tomography (CT), magnetic resonance imaging (MRI), and ultrasound (US) imaging. X-ray CT is the mass screening tool for detecting radiopaque foreign bodies. However, it has obvious drawbacks. Repeated x-ray exposure can be harmful to the human body despite using low doses of radiation. Most importantly, x-ray contrast is not appropriate for detecting radiolucent substances, such as wood, cloth, and plastic. MRI is increasingly used as a complementary alternative. It can give superior soft-tissue contrast compared to other imaging methods. However, MRI is not suitable for detecting metallic fragments because it gives rise to strong interference artifacts.³ It may also present potential hazards for the patient due to magnetically induced movement of the metallic object through the soft tissues.⁴ Other disadvantages of MRI include limited spatial resolution and high cost. US imaging is widely used in clinics because of its real-time display, zero ionizing radiation exposure, and affordable price. Unfortunately, it suffers from poor sensitivity (52.6%) and specificity (47.2%) in detecting small foreign bodies.⁵ Moreover, distinguishing vital from nonvital tissues in wounds is challenging. Photoacoustic (PA) imaging, however,

can image blood vessels and functions without extrinsic contrast agents at high resolution and can image much deeper than other optical technologies.^{6–8} Imaging of the wound areas can potentially be made real time. The wavelength tuning capability helps identification of debris types.

2 Materials and Methods

2.1 Photoacoustic Imaging System

A deep reflection mode PA imaging system was used.⁹ Figure 1 shows the schematic of the system. Upon laser excitation, the tissue generates ultrasonic waves, known as PA waves. The PA waves were first received by an ultrasonic transducer, amplified by a pulser/receiver (5072PR, Panametrics-NDT, Watham, Maryland), digitized by an oscilloscope (Tektronix TDS 5054, Natham, Massachusetts) and stored in a computer, which also controlled an XY-linear translation stage (XY-6060, Danaher Motion, Washington, DC) for raster scanning. A photodiode (SM05PD1A, Thorlabs, Newton, New Jersey) was used to compensate for the energy instability of laser pulses.

To achieve deep penetration of light, a tunable near-infrared Ti:sapphire laser (LT-2211A, LOTIS TII, Minsk, Belarus) pumped by a Q-switched Nd:YAG laser (LS-2137/2, LOTIS TII, Minsk, Belarus) was used for PA excitation. The laser pulse duration was <15 ns, and the repetition rate was 10 Hz. The incident laser beam on the tissue surface was controlled to be less than the ANSI standard for maximum permissible exposure (31 mJ/cm²).¹⁰

To receive deep PA signals with minimal ultrasonic attenuation, a 5-MHz central frequency ultrasonic transducer (V308, Panametrics-NDT, Watham, Maryland) was used. This transducer had a spherical focus with a 2.54-cm focal length, a 1.91-cm active diameter, and a 72% nominal bandwidth based on the full width at half maximum amplitudes. The spatial resolutions

*Current address: University of Buffalo, State University of New York, 328 Bonner Hall, Buffalo, New York 14260.

Address all correspondence to: Lihong V. Wang, Washington University in St. Louis, Department of Biomedical Engineering, Optical Imaging Laboratory, St. Louis, Missouri 63130. Tel: 314-935-6152; Fax: 314-935-7448; E-mail: lhwang@biomed.wustl.edu.

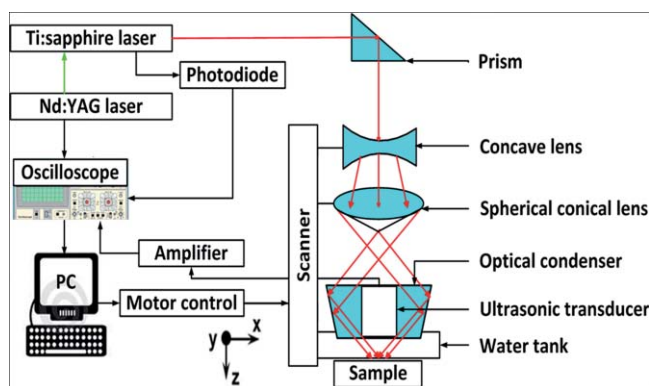


Fig. 1 Schematic of the deep-penetrating reflection-mode photoacoustic imaging system. A Cartesian coordinate is shown.

were $144\ \mu\text{m}$ in the axial direction and $560\ \mu\text{m}$ in the transverse direction. The scanning time depends on the laser pulse repetition rate, the scanning step size, and the field of view. Typical values are a 0.1-mm scanning step size for a 1-D scan and a 10-Hz laser pulse repetition rate. The acquisition time is ~ 6 s for a B-scan. Note that the signal was not averaged for any of the images. The transducer was located inside a water container with an opening of 5×5 cm at the bottom, sealed with a thin, clear polyethylene membrane. The object was placed under the membrane, and ultrasonic gel was used for US coupling. To reduce the surface PA wave generation, a concave lens, a spherical conical lens, and an optical condenser were used to form the dark-field illumination.¹¹

2.2 Ultrasound Imaging System

With some slight modifications to the PA imaging system, we can get coregistered pulse-echo US images with the PA images. A function generator (33250A, Agilent, Santa Clara, California) instead of the laser was used as the trigger source. The pulser/receiver (5072PR, Panametrics-NDT, Watham, Maryland) was set to transmit/receive mode for pulse echo transmission and detection. For this study, another clinical US imaging system (iU22; Philips Healthcare, Andover, Massachusetts) with a linear-array (L8-4, 128 elements, 4–8 MHz) was used for comparison to PA images as well.

2.3 Sample Preparation

Chicken breast tissue was used as the background medium mimicking the human soft tissue.¹² Pieces of foreign bodies with arbitrary shapes were embedded in the chicken breast tissue at depths ranging from 3 to 10 mm. A metal blade, a piece of plastic, a piece of wood, a piece of cloth, and a piece of glass were used to test the ability of PA imaging to detect foreign bodies. Also, two pieces of wood, two pieces of cloth, and a piece of plastic were used for a comparison between PA imaging and US imaging. Then, a piece of wood and a piece of cloth were used for spectroscopic PA imaging.

3 Results

3.1 Photoacoustic Ability to Detect Foreign Bodies

To show the feasibility of PA imaging of foreign bodies, we imaged various foreign bodies embedded in chicken tissue using

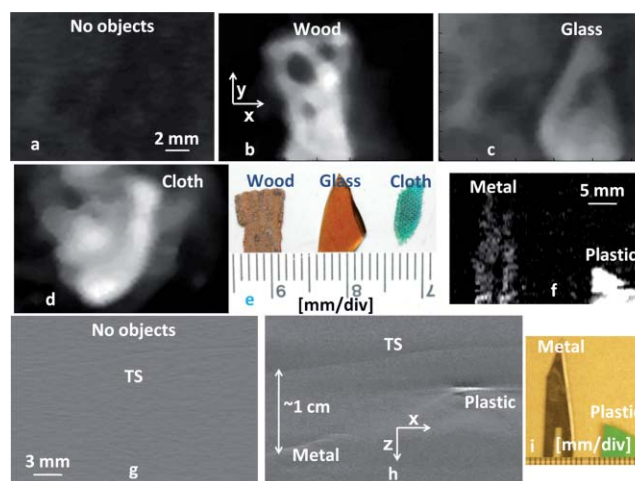


Fig. 2 PA images and digital photographs for various foreign bodies. Objects were embedded in chicken breast tissue: (a) PA MAP image without objects embedded in the tissue, (b–d,f) PA MAP images, (e,i) digital photographs, (g) PA B-scan image without objects embedded in the tissue, and (h) PA B-scan images. TS: tissue surface.

an optical wavelength of 766 nm. We could clearly see the objects in the PA images. Figures 2(a) and 2(g) show the PA maximum amplitude projection (MAP) and B-scan without any objects embedded in the tissue, respectively. We do not see anything. Figures 2(b)–2(d) show the PA MAP images of a piece of wood, a piece of glass, and a piece of cloth. Figure 2(f) shows the PA MAP images of a piece of metal and a piece of plastic. MAP was performed by projecting the maximum signal amplitude from each A-line onto the XY plane. The shapes of the objects agree well with those of the actual samples shown in Figs. 2(e) and 2(i). Figure 2(h) shows the B-scan image of the piece of metal and piece of plastic. Imaging depth can reach >1 cm. The results indicate that PA is excellent for exactly locating the foreign bodies of various debris materials.

3.2 Comparison to Ultrasound Imaging

US is not sensitive to tiny objects (a few millimeters) because of their low acoustic contrasts or because of operator variability, especially in the presence of ubiquitous US speckles.¹³ By contrast, PA imaging provides excellent optical absorption contrast and US spatial resolution, enabling detection of tiny objects. To show this advantage of PA imaging, PA imaging and US imaging were compared. A piece of wood and a piece of cloth were embedded in chicken breast tissue and were imaged by both the PA system and the clinical US system. Then, they were cut to smaller sizes and were imaged again by both imaging modalities. Figures 3(a) and 3(f) show digital photographs for the samples. Figures 3(b) and 3(c) show the PA B-scan images of the larger wood and larger cloth, respectively. Figures 3(d) and 3(e) show the US B-scan images of the larger wood and larger cloth, respectively. Figures 3(g) and 3(h) show the PA B-scan images of the smaller wood and smaller cloth, respectively. Figures 3(i) and 3(j) show the US B-scan images of the smaller wood and the smaller cloth, respectively. Although both modalities successfully imaged the objects, PA images had much higher contrasts than US images. The contrast is defined as $(I - I_b)/I_b$ with I and I_b representing the average signal intensity of the foreign body

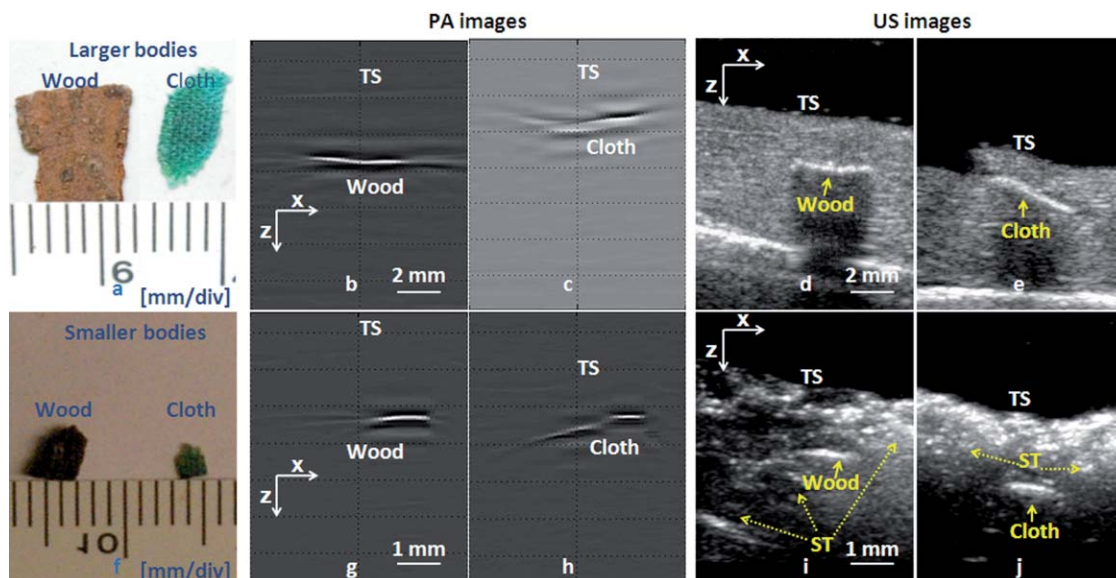


Fig. 3 PA and US B-scan images of foreign bodies of two sizes. Objects were embedded in chicken breast tissue: (a,f) Digital photographs, (b,c) PA B-scan images of the larger foreign bodies, (d,e) US B-scan images of the larger foreign bodies, (g,h) PA B-scan images of the smaller foreign bodies and (i,j) US B-scan images of the smaller foreign bodies. TS: tissue surface; ST: surrounding tissue.

and that of the background (chicken breast tissue), respectively. The PA contrasts of the larger wood and larger cloth are ~ 11 and ~ 13 , respectively, whereas the corresponding US contrasts are only ~ 1.2 and ~ 1.5 , respectively. Moreover, after the targets were cut, the PA contrasts of the wood and cloth remained almost the same, but the corresponding US contrasts were reduced to only ~ 0.6 and ~ 0.7 , respectively. The poor US contrasts made it difficult to identify the smaller foreign bodies in US images.

US specificity is limited by the overlapping acoustic characteristics of foreign bodies and the surrounding tissue.¹⁴ If the foreign bodies have low optical absorption contrast but sufficient acoustic contrast, they may show up in US images but not in PA images. Therefore, PA imaging and US imaging are complementary and will not supplant each other. However, PA images and US images can be acquired from the same cross sections of the sample.^{15–18} The two types of images can be coregistered naturally to combine the advantages of PA and US imaging. As shown in Fig. 4, a piece of dark soft polyethylene plastic (thickness, $\sim 150 \mu\text{m}$) buried in chicken breast tissue was detected by coregistered images. In the PA images shown in Figs. 4(a) and 4(d), the location and size of the target were accurately specified. It is not showing up in the coregistered US MAP and B-scan images [Figs. 4(b) and 4(e)] because the piece of plastic has a similar acoustic property with the tissue. As shown in Fig. 4(f), the clinical US system cannot detect the piece of plastic either.

3.3 Spectroscopic PA Imaging

For spectroscopic PA study, we used the same Ti:sapphire laser with the wavelength ranging from 750 to 800 nm, and the other parameters are the same as those used in the previous PA experiments. Figure 5 shows the PA spectra of a piece of green cloth and a piece of brown wood. To validate the results, the optical absorbance of the corresponding color ink was acquired by a spectrophotometer (Cary 50 Bio, Varian, Walnut Creek, California). Each curve was normalized by its own minimum

value. The correlation coefficients between the PA curve and the absorbance curve in Figs. 5(a) and 5(b) are 0.82 and 0.92, respectively. Spectral analysis would be helpful in choosing the optimal light wavelengths for imaging specific objects to produce high-contrast images. In addition, viable and nonviable tissue can potentially be distinguished spectrally.¹⁹

4 Discussions and Conclusion

We have demonstrated that PA imaging can be used as a tool to detect foreign bodies in biological tissue. PA imaging is sensitive to intrinsic and extrinsic optical contrasts. In addition, it is relatively inexpensive and portable. Therefore, photoacoustic

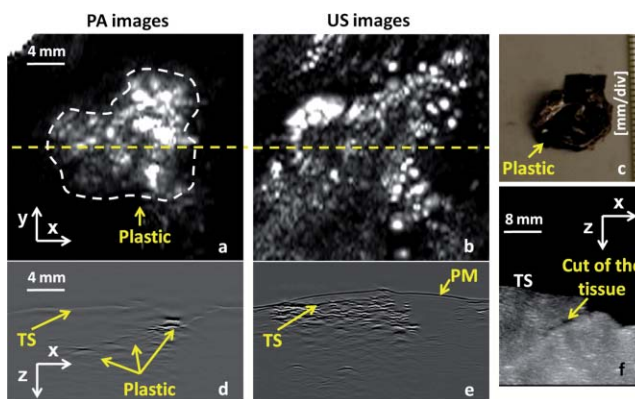


Fig. 4 Coregistered PA and US images for a piece of plastic. The object was embedded in chicken breast tissue: (a) Photoacoustic MAP image (signals from the tissue surface were removed), (b) coregistered US MAP image (signals from the tissue surface and from the polyethylene membrane were removed), (c) digital photograph, (d) B-scan image of (a) at the dashed line, (e) B-scan image of (b) at the dash line, and (f) B-scan image acquired by the clinical US system. TS: tissue surface; PM: polyethylene membrane.

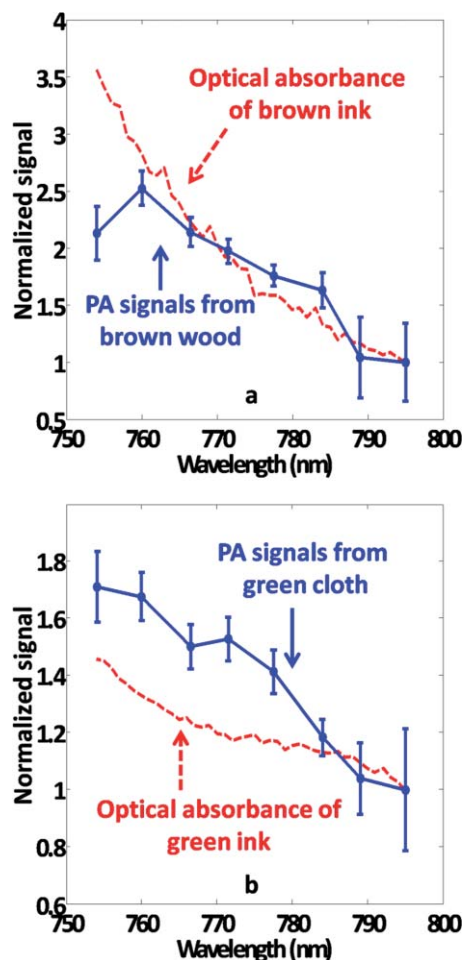


Fig. 5 Optical absorption spectra of foreign bodies measured by PA imaging. (a) PA amplitude of the brown wood and optical absorbance of brown ink versus the optical wavelength. (b) PA amplitude of the green cloth and optical absorbance of green ink versus the optical wavelength.

imaging can potentially be useful in intraoperative procedures for debris detection and removal.

US imaging is widely used in the clinic because of its real-time display, nonionizing radiation exposure, and low cost. US elastography can potentially improve the visibility of foreign objects. Of course, PA imaging also has its limitations. It is difficult to detect transparent or low optical absorption foreign bodies, which may show up as negative contrasts in PA images. Overall, PA and US images have complementary contrasts and can be naturally coregistered. Coregistered images of the sample can potentially increase the sensitivity and specificity for detecting foreign bodies.

Acknowledgments

We are grateful to Todd N. Erpelding for experimental assistance. This work was sponsored by National Institutes of Health Grant Nos. R01 EB000712, R01 EB008085, R01 CA134539,

and U54 CA136398 (Network for Translational Research). L.V.W. has a financial interest in Microphotoacoustics, Inc. and Endra, Inc., which, however, did not support this work.

References

1. R. L. Lammers, "Soft tissue foreign bodies," *Ann. Emerg. Med.* **17**, 1336–1347 (1988).
2. Walter Reed Army Medical Center, *Emergency War Surgery*, 3rd U.S. rev., Walter Reed Army Medical Center, Washington DC (2004).
3. P. J. Holmes, J. R. Miller, R. Gutta, and P. J. Louis, "Intraoperative imaging techniques: A guide to retrieval of foreign bodies," *Oral Surg., Oral Med., Oral Pathol., Oral Radiol. Endodontology*. **100**, 614–618 (2005).
4. B. Cakir, M. Atkan, S. Yildirim, and T. Akoz, "Localization and removal of ferromagnetic foreign bodies by magnet," *Ann. Plast. Surg.* **49**, 541–544 (2002).
5. C. S. Crystal, D. A. Masneri, J. S. Hellums, D. W. Kaylor, S. E. Young, M. A. Miller, and M. E. Levsky, "Bedside ultrasound for the detection of soft tissue foreign bodies: A cadaveric study," *J. Emerg. Med.* **36**(4), 377–380 (2009).
6. H. F. Zhang, K. Maslov, G. Stoica, and L. V. Wang, "Functional photoacoustic microscopy for high-resolution and noninvasive *in vivo* imaging," *Nat. Biotechnol.* **24**(7), 848–851 (2006).
7. C. Kim, C. Favazza, and L. V. Wang, "In vivo photoacoustic tomography of chemicals: High-resolution functional and molecular optical imaging at new depths," *Chem. Rev.* **110**(5), 2756–2782 (2010).
8. L. V. Wang, "Multiscale photoacoustic microscopy and computed tomography," *Nat. Photon.* **3**(9), 503–509 (2009).
9. K. H. Song and L. V. Wang, "Deep reflection-mode photoacoustic imaging of biological tissue," *J. Biomed. Opt.* **12**(6), 060503 (2007).
10. American National Standards Institute, "American national standard for the safe use of lasers," ANSI Z136.1-2000, American National Standards Institute, New York (2000).
11. K. Maslov, G. Stoica, and L. V. Wang, "In vivo dark-field reflection-mode photoacoustic microscopy," *Opt. Lett.* **30**(6), 625–627 (2005).
12. G. Marquez, L. V. Wang, S. P. Lin, J. A. Schwartz, and S. L. Thomsen, "Anisotropy in the absorption and scattering spectra of chicken breast tissue," *Appl. Opt.* **37**, 798–805 (1998).
13. A. Fenster, D. B. Downey, and H. N. Cardinal, "Three-dimensional ultrasound imaging," *Phys. Med. Biol.* **46**, R67–R99 (2001).
14. C. D. Lehman, C. Isaacs, M. D. Schnall, E. D. Pisano, S. M. Ascher, P. T. Weatherall, D. A. Bluemke, D. J. Bowen, P. K. Marcom, D. K. Armstrong, S. M. Domchek, G. Tomlinson, S. J. Skates, and C. Gatsonis, "Cancer yield of mammography, MR, and US in high-risk women: Prospective multi-institution breast cancer screening study," *Radiology* **244**(2), 381–388 (2007).
15. T. N. Erpelding, C. Kim, M. Pramanik, L. Jankovic, K. Maslov, Z. Guo, J. A. Margenthaler, M. D. Pashley, and L. V. Wang, "Sentinel lymph nodes in the rat: Noninvasive photoacoustic and US imaging with a clinical US system," *Radiology* **256**(1), 102–110 (2010).
16. C. Kim, T. N. Erpelding, K. Maslov, L. Jankovic, W. J. Akers, L. Song, S. Achilefu, J. A. Margenthaler, M. D. Pashley, and L. V. Wang, "Handheld array-based photoacoustic probe for guiding needle biopsy of sentinel lymph nodes," *J. Biomed. Opt.* **15**(4), 046010 (2010).
17. J. J. Niederhauser, M. Jaeger, R. Lemor, P. Weber, and M. Frenz, "Combined ultrasound and photoacoustic system for real-time high-contrast vascular imaging *in vivo*," *IEEE Trans. Med. Imaging* **24**(4), 436–440 (2005).
18. R. G. Kolkman, P. J. Brands, W. Steenbergen, and van T. G. Leeuwen, "Real-time *in vivo* photoacoustic and ultrasound imaging," *J. Biomed. Opt.* **13**(5), 050510 (2008).
19. H. F. Zhang, K. Maslov, M. Sivaramakrishnan, G. Stoica, and L. V. Wang, "Imaging of hemoglobin oxygen saturation variations in single vessels *in vivo* using photoacoustic microscopy," *Appl. Phys. Lett.* **90**(5), 053901 (2007).